



Cite this: DOI: 10.1039/c7tc02925j

## Structure–property relationship of D–A type copolymers based on phenanthrene and naphthalene units for organic electronics†

Yeong-A Kim,<sup>a</sup> Minji Kang,<sup>a</sup> Ye-Jin Jeon,<sup>a</sup> Kyeongil Hwang,<sup>a</sup> Yeon-Ju Kim,<sup>a</sup> Soo-Young Jang,<sup>‡a</sup> In-Bok Kim,<sup>b</sup> Gucheol Kwon<sup>a</sup> and Dong-Yu Kim<sup>ib</sup> \*<sup>ab</sup>

Four donor–acceptor (D–A) type conjugated polymers (**PA1**, **PA2**, **PA3** and **PA4**) based on phenanthrene and naphthalene as the donating units with or without dimethoxy substitution were synthesized for organic field effect transistors (OFETs) and bulk-heterojunction organic photovoltaics (OPVs). Dimethoxy substituents have significant effects on the optical, electrochemical, charge transport and photovoltaic properties depending on the donor–polyaromatic (PA) compounds. The optical band gaps of these PA-based copolymers from the smallest to the largest are as follows: 1.52 eV (1,5-dimethoxy substituted naphthalene (**PA4**)), 1.59 eV (unsubstituted naphthalene (**PA3**)), and 1.63 eV (unsubstituted phenanthrene (**PA1**), and substituted 9,10-dimethoxy phenanthrene (**PA2**)). While the values vary depending on the compounds, both **PA2** and **PA4** are found to have higher highest occupied molecular orbital (HOMO) energy levels than those of **PA1** and **PA3** due to the electron donating nature of dimethoxy substituents. The PA based copolymers without dimethoxy substituents showed highly balanced ambipolar behavior with  $\sim 1 \text{ cm}^2 \text{ V}^{-1} \text{ s}^{-1}$ , whereas the electron mobility of dimethoxy modified PA (MeOPA) based copolymers was suppressed. The inverted bulk heterojunction OPVs based on **PA1** and **PA3** exhibited power conversion efficiency (PCE) as high as 5.3% and 5.8%, respectively. The PCEs of PA copolymer-based OPV devices were mainly affected by an increase in the open circuit voltage rather than by the photocurrent or fill factor.

Received 29th June 2017,  
Accepted 19th September 2017

DOI: 10.1039/c7tc02925j

rsc.li/materials-c

## Introduction

Organic electronics including organic field effect transistors (OFETs) and organic photovoltaics (OPVs) using conjugated polymers as organic semiconducting materials have attracted wide interest in recent years because of their advantages such as low production cost, low weight, mechanical flexibility, and solution processibility.<sup>1–7</sup> Furthermore, conjugated polymers can also be processed easily over a large-area device and their electronic properties can be easily tuned through diversification of the chemical structures. Although the device performance is

affected by many factors such as device architectures, processing conditions, and choice of electrodes, the importance of molecular design for a polymer structure is evident as a determining factor for high performance.<sup>8–11</sup>

As semiconducting materials for OFETs, conjugated polymers are required to have several important properties.<sup>12</sup> First,  $\pi$ -orbitals should be well-overlapped through the conjugated backbone of polymers for efficient charge transport. To obtain high carrier mobilities, both intramolecular charge transport in the conjugated backbone and intermolecular charge transport between the adjacent molecules need to be maximized. In this regard, polymers need to adopt a coplanar conjugated backbone structure for efficient intramolecular charge transport and favorable orientation of polymer chains for strong intermolecular interaction between the neighboring polymer molecules.<sup>13–15</sup> Second, energy levels of polymers should be matched with the work functions of electrodes in order to minimize the energy barrier for charge injection. While many studies of p-type semiconducting materials have been published reporting high mobilities, research on n-type and ambipolar materials is relatively lagging.<sup>1,16</sup> For n-type or ambipolar characteristics, a low-lying lowest unoccupied molecular orbital (LUMO) level is necessary for adequate electron

<sup>a</sup> School of Materials Science & Engineering, Gwangju Institute of Science and Technology (GIST), 123 Cheomdangwagi-ro, Buk-gu, Gwangju 61002, Republic of Korea

<sup>b</sup> Research Institute for Solar and Sustainable Energies (RISE), Gwangju Institute of Science and Technology (GIST), 123 Cheomdangwagi-ro, Buk-gu, Gwangju 61002, Republic of Korea. E-mail: kimdy@gist.ac.kr

† Electronic supplementary information (ESI) available. See DOI: 10.1039/c7tc02925j

‡ Current address: Department of Chemistry and Centre for Plastic Electronics, Imperial College London, Exhibition Rd, London, SW7 2AZ, UK. E-mail: s.jang@imperial.ac.uk

injection. In addition, environmental, electrical, and thermal stability is required for the overall operational stability of the device.

Furthermore, for achieving high performance in bulk heterojunction (BHJ) OPVs, conjugated polymers as donor materials have to be designed to satisfy several requirements. The power conversion efficiency (PCE) of photovoltaics is determined by the open circuit voltage ( $V_{oc}$ ), the short-circuit current ( $J_{sc}$ ), and the fill factor (FF). These factors can be controlled by varying the chemical structure of polymers.<sup>17,18</sup> The value of  $V_{oc}$  is mainly affected by the energy levels of donor materials. The most widely used acceptor material for OPVs is [6,6]-phenyl-C<sub>71</sub>-butyric acid methyl ester (PC<sub>71</sub>BM). When PC<sub>71</sub>BM is employed,  $V_{oc}$  increases proportionally as a function of the difference between the highest occupied molecular orbital (HOMO) energy level of a polymer and the LUMO energy level of PC<sub>71</sub>BM.<sup>19–21</sup> The value of  $J_{sc}$  is influenced by the amount of photon absorption and exciton dissociation.<sup>22,23</sup>  $J_{sc}$  can be improved by lowering the optical band gap of a polymer which results in a broader absorption in the solar spectrum.<sup>24</sup> In addition, donor materials are required to have high hole mobility in order to obtain a reasonable FF.<sup>25</sup>

To achieve high device performance, conjugated polymers have to be carefully designed in accordance with the above requirements. Therefore, the HOMO energy level of a polymer material should be lowered and the optical energy band gap of the polymer should be lowered in order to obtain high  $V_{oc}$  and  $J_{sc}$  in OPVs.<sup>21</sup> To meet these requirements, we reported donor–acceptor (D–A) type conjugated copolymers with different solubilizing groups based on 9,10-alkoxy phenanthrene and diketopyrrolopyrrole (DPP) units, one kind of strong acceptor, depending on a “weak donor–strong acceptor design” strategy.<sup>26–33</sup> Incorporation of phenanthrene units as weak donor units into conjugated backbones led to a deep HOMO energy level for high  $V_{oc}$  and introducing a kind of strong acceptor, the DPP unit, induced low band gap properties for high photocurrent.<sup>34</sup>

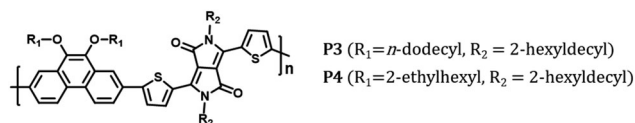
Although phenanthrene molecules comprising three-fused benzene rings have the potential to be a good candidate as electron donating units, the previously reported device performance of (phenanthrene-*alt*-diketopyrrolopyrrole) PDPP copolymers was poor.<sup>35,36</sup> The copolymers with a longer alkoxy side chain on phenanthrene showed a worse device performance compared to their counterpart polymers. In addition, the conjugated polymers containing DPP units are known to have limited solubility which could result in low molecular weight of the polymers in the absence of a long and bulky side chain due to their strong intermolecular interactions.<sup>37–42</sup> In our previous study, we confirmed that an alkoxy side chain on phenanthrene should be shorter and an alkyl side chain on DPP units should be longer in order to improve polymer solubility without sacrificing the optoelectronic properties.<sup>34</sup> Similarly, research about PDPPT–NAP based on dodecyloxy naphthalene and DPP was reported by Sonar P. *et al.* PDPPT–NAP showed p-type characteristics with the highest hole mobility of around 0.0046 cm<sup>2</sup> V<sup>-1</sup> s<sup>-1</sup>.<sup>43</sup>

In this work, we synthesized a series of D–A copolymers containing four different polyaromatic (PA) compounds as D

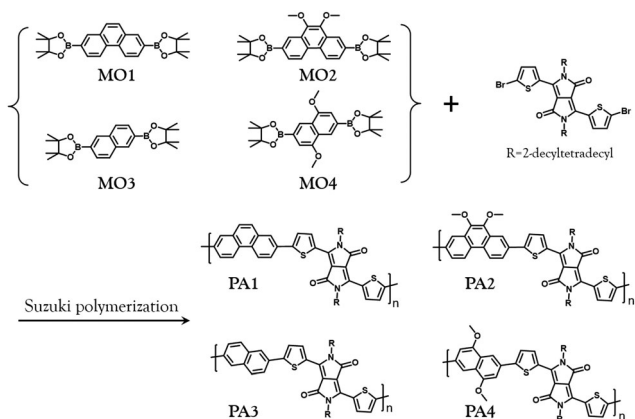
units and a DPP unit with 2-decyltetradecyl chains as an A unit. The PA compounds which are introduced in this study are as follows: unsubstituted phenanthrene (for **PA1**), 9,10-dimethoxy, shortest alkoxy chain, substituted phenanthrene (for **PA2**), unsubstituted naphthalene (for **PA3**), and 1,5-dimethoxy substituted naphthalene (for **PA4**). These PA-based copolymers were synthesized *via* Suzuki polymerization, as represented in Scheme 2.

## Results and discussion

The chemical structures of the four (MeO)PA–DPP copolymers are represented in Scheme 1. **MO1**, **MO2**, **MO3**, **MO4** and **DTDPP** were synthesized using the same procedure followed in the literature, and specific synthetic steps are depicted in Fig. S1 (ESI<sup>†</sup>).<sup>44–47</sup> Poly{phenanthrene-2,7-diyl-*alt*-3,6-dithiophene-2-yl-2,5-di(2-decyltetradecyl)-pyrrolo[3,4-*c*]pyrrole-1,4-dione} (**PA1**), poly{9,10-dimethoxyphenanthrene-2,7-diyl-*alt*-3,6-dithiophene-2-yl-2,5-di(2-decyltetradecyl)-pyrrolo[3,4-*c*]pyrrole-1,4-dione} (**PA2**), poly{naphthalene-2,6-diyl-*alt*-3,6-dithiophene-2-yl-2,5-di(2-decyltetradecyl)-pyrrolo[3,4-*c*]pyrrole-1,4-dione} (**PA3**) and poly{1,5-dimethoxynaphthalene-3,7-diyl-*alt*-3,6-dithiophene-2-yl-2,5-di(2-decyltetradecyl)-pyrrolo[3,4-*c*]pyrrole-1,4-dione} (**PA4**) were synthesized *via* Suzuki polymerization. The resulting polymers showed good solubility in chloroform and poor solubility in chlorobenzene, *o*-dichlorobenzene and toluene. However, **PA4** has somewhat lower molecular weight than the other polymers due to its low solubility. All polymers exhibited excellent thermal stability with a decomposition temperature ( $T_d$ ) of up to 412, 385, 417 and 409 °C for **PA1**, **PA2**, **PA3**, and **PA4**, respectively. On DSC measurement, they did not show any thermal transition between 40 °C and 300 °C (Fig. S2 and S3, ESI<sup>†</sup>).



Scheme 1 Chemical structure of **P3** and **P4**.<sup>34</sup>



Scheme 2 Synthetic scheme and chemical structures of (MeO)PA–DPP copolymers.

## Theoretical calculations

Density functional theory (DFT) was employed for computational studies of the effect of dimethoxy substitution on molecular geometries and electronic wave functions of the frontier orbitals in the four conjugated systems. Computations were performed using the respective trimers of each copolymer with Gaussian 09 at the B3LYP/6-311G(d,p) level of theory. The optimized geometries of all compounds are shown in Fig. S4 (ESI<sup>†</sup>). All (MeO)PA-based copolymers showed a fairly twisted structure due to a large dihedral angle ( $\varphi$ ) between PA compounds and thiophene units. The respective dihedral angles between the (MeO)PA unit and DPP unit of each polymer were 25.1°, 25.1°, 24.9°, and 25.66° for **PA1**, **PA2**, **PA3**, and **PA4**, respectively (Scheme 3).

In Fig. S5 (ESI<sup>†</sup>), these polymers showed a slight difference in both HOMO and LUMO distribution. The orbital distributions of phenanthrene-based polymers, **PA1** and **PA2**, are rather strongly localized within the DPP units and remain similar regardless of dimethoxy substituents. Therefore, dimethoxy substituents make minor contributions to either the HOMO or LUMO of phenanthrene units. On the other hand, the electron density of **PA3** is relatively localized similar to that of phenanthrene-based polymers, but the HOMO of **PA4** is distributed over the entire conjugated backbone. The introduction of dimethoxy substituents at the 1,5-position of naphthalene highly affected the HOMO energy levels of the polymers relative to those of the 9,10-dimethoxy phenanthrene units, which could be caused by their different mesomeric (resonance) structures.

The lone pair electrons of the oxygen atom in the methoxy substituent can be released toward the PA rings and can be delocalized through the conjugated system. Thus the electron density of MeOPA is higher than PA without dimethoxy

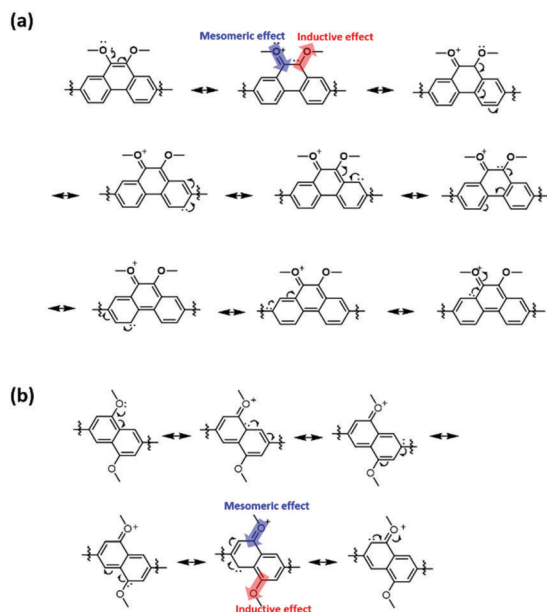
substituents due to the positive mesomeric effect of methoxy groups. However, methoxy groups can also weakly withdraw the electrons through the  $\sigma$  bond due to higher electronegativity of the oxygen atom and induce a fractional positive charge ( $\delta^+$ ) in the aromatic carbon, called a negative inductive effect. As can be seen in Fig. S5 (ESI<sup>†</sup>), the conjugation system of **PA2** containing 9,10-dimethoxyphenanthrene showed a similar distribution of the HOMO level to those of the unsubstituted polymer, **PA1**. When the lone pair electrons are donated owing to the mesomeric effect, it could be stabilized through the electron-withdrawing inductive effect by the adjacent oxygen atom. However, in the case of naphthalene derivatives, **PA4**, dimethoxy groups are substituted in opposite directions. Such placement of two methoxy substituents makes non-pair electrons from the oxygen atom well delocalized over the  $\pi$ -conjugated system.<sup>48</sup>

Dimethoxy substituents on the PA units had a stronger effect on the HOMO than on the LUMO energy level of copolymers. A similar trend was observed for (MeO)PA-DPP copolymers for the LUMO distribution localized on the DPP units. The calculated HOMO/LUMO energies were  $-5.04/-2.89$ ,  $-4.99/-2.85$ ,  $-5.01/-2.94$ , and  $-4.82/-2.79$  eV for **PA1**, **PA2**, **PA3**, and **PA4**, respectively.

## Optical properties

Normalized absorption spectra of the (MeO)PA copolymers in both *o*-dichlorobenzene solution and thin films are shown in Fig. 1. Both in solution and in thin films, (MeO)PA-DPP copolymers have two-band absorption spectra with a weak intensity band at shorter wavelengths (300–500 nm) attributed to localized  $\pi$ - $\pi^*$  electron transitions and with relatively strong absorption at a longer-wavelength (500–800 nm) arising due to internal charge transfer (ICT) between electron-rich polyaromatic units and electron-deficient DPP units. All (MeO)PA based copolymers showed a significant vibronic peak which comes from the strong interchain  $\pi$ - $\pi$  stacking and intermolecular packing of polymer molecules even in the solution state at room temperature. Temperature-dependent absorption spectra of (MeO)PA copolymers in *o*-dichlorobenzene were examined by increasing the temperature from 40 °C to 110 °C (Fig. S7, ESI<sup>†</sup>). We observed hypsochromic shifts in absorption spectra and weaker vibronic peaks at higher temperatures. However, **PA1**, **PA2**, and **PA3** showed similar trends in absorption spectra with intense aggregation even at 110 °C which is likely due to a strong intermolecular interaction among their polymer chains. By contrast, in **PA4**, the shoulder peak ( $\lambda_{\text{max}} = 740$  nm at 40 °C) was suppressed and largely hypsochromically shifted from 740 nm to 721 nm due to disaggregation of polymer chains and steric repulsion upon heating.

As shown in Fig. 1b, the absorption spectra of polymer thin films are broader than those of polymer solutions due to the strong intermolecular interaction. In addition, the absorption spectra of **PA1**, **PA2**, **PA3** and **PA4** films have absorption maxima ( $\lambda_{\text{max}}$ ) at 705, 702, 724, and 754 nm, respectively while their optical band gaps that were measured from the absorption onset were 1.63 eV, 1.63 eV, 1.59 eV, and 1.52 eV, respectively.



**Scheme 3** Mesomeric structure of (a) 9,10-dimethoxyphenanthrene and (b) 1,5-dimethoxynaphthalene.

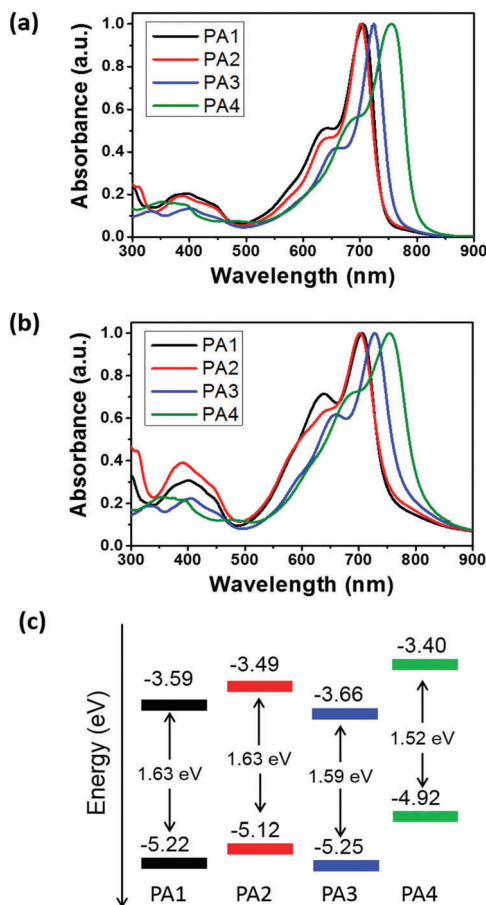


Fig. 1 UV-vis absorption spectra of (MeO)PA-DPP copolymers (a) in *o*-dichlorobenzene solution and (b) in films. (c) Schematic energy diagrams of (MeO)PA-DPP copolymers.

Interestingly, the absorption spectrum of **PA2** was similar to that of **PA1** regardless of the dimethoxy groups at the 9,10-position of phenanthrene, while **PA4** exhibited an optical behaviour, which was quite different from that of **PA3**. The absorption spectrum of **PA4** was fairly red-shifted, and **PA4** had the lowest band gap caused by efficient ICT. With the acceptor strength being equal, 1,5-dimethoxy substituted naphthalene is possibly the donor with the strongest electron donating ability among the four samples studied based on band-gap measurements.<sup>49,50</sup>

### Electrochemical properties

Cyclic voltammetry (CV) was employed to investigate the electrochemical properties of PADPP copolymers. CV was performed in 0.1 M tetrabutylammonium perchlorate ( $\text{Bu}_4\text{NClO}_4$ ) and calibrated with ferrocene/ferrocenium as a reference. The HOMO energy levels of polymers were derived from the following equation.

$$E_{\text{HOMO}} = [(E_{\text{ox}} - E_{1/2}(\text{ferrocene})) + 4.8] \text{ eV}$$

Here,  $E_{\text{ox}}$  and  $E_{1/2}(\text{ferrocene})$  are the onset of oxidation potential of a polymer and half-wave potential of ferrocene, respectively.

For  $E_{1/2}(\text{ferrocene}) = 0.42 \text{ V}$ , the HOMO energy levels of **PA1**, **PA2**, **PA3**, and **PA4** are equal to  $-5.22$ ,  $-5.12$ ,  $-5.25$ , and  $-4.92 \text{ eV}$ , respectively. With the exception of **PA4**, the polymers have low-lying HOMO energy levels indicating that they could have high  $V_{\text{oc}}$  in OPVs because  $V_{\text{oc}}$  is mainly determined by the difference between the HOMO energy level of the polymer and the LUMO energy level of the acceptor. The LUMO energy levels are calculated from the optical band gap and the HOMO energy level as  $-2.89$ ,  $-2.85$ ,  $-2.94$ , and  $-2.82 \text{ eV}$  for **PA1**, **PA2**, **PA3**, and **PA4**, respectively. The difference between the LUMO levels of the polymers and the LUMO level of PC<sub>71</sub>BM is sufficient for efficient exciton dissociation.<sup>50,51</sup> **PA1** and **PA3** with unsubstituted PA compounds have higher oxidation potential than dimethoxy substituted PA based copolymers. Two methoxy substituents induce different electronic effects in phenanthrene and naphthalene.

The same as the *meta*- and *para*-substituted alkoxy groups on benzene have different influences on electronic effects, **PA2** and **PA4** do not have the same energy levels because of their different mesomeric structures.<sup>52</sup> In the case of 9,10-dimethoxy phenanthrene, methoxy substituents are in immediate proximity to each other and they cannot donate their non-bonding electrons to the conjugated backbone simultaneously. While the oxygen atom can donate its unpaired electron through the mesomeric effect to the conjugated backbone, electrons can also be pulled again by an electron withdrawing inductive effect due to the high electronegativity of oxygen. Thus, **PA2** showed a slightly higher HOMO energy level than **PA1** with a difference of about 0.1 eV. In contrast, the HOMO energy level of 1,5-dimethoxy substituted naphthalene-based polymer, **PA4**, is much higher compared to that of **PA3** due to a strong resonance effect through naphthalene units.

### Thin-film microstructure analysis

Tapping-mode atomic force microscopy (AFM) analysis was carried out for the investigation of the influence of (MeO)PA units on thin film morphologies, and AFM images of each polymer film on a glass substrate are shown in Fig. S9 (ESI†). All polymer films were spin-coated and then thermally treated with a temperature selected to optimize the OFET device performance. The pristine films of (MeO)PA-based copolymers formed fine fibrillar structures with root-mean-square (rms) roughness values of 1.33, 0.52, 0.91, and 2.81 nm for **PA1**, **PA2**, **PA3**, and **PA4**, respectively. Thermally annealed polymer films formed fibrillar aggregates with higher rms roughness, making the enhancement of intermolecular interactions feasible for efficient charge transport (Table 1).

Grazing-incidence wide-angle X-ray scattering (GIWAXS) analysis of neat polymer films was performed to obtain information on the order and molecular stacking mode of the polymer films. The X-ray diffraction (XRD) profiles of the pristine and thermally annealed films at the optimum temperature for the OFET devices are shown in Fig. 2. **PA1** and **PA3** showed (*h*00) diffraction that is related to lamella *d*-spacing up to the fourth order peak even in pristine films in the out-of-plane direction, indicating a highly ordered and crystalline structure with an edge-on orientation. After thermal treatment, (MeO)PA

Table 1 Photophysical and electrochemical properties

Polymer	$\lambda_{\text{max}}^{\text{solution}}$ (nm)	$\lambda_{\text{max}}^{\text{film}}$ (nm)	$\lambda_{\text{onset}}^{\text{film}}$ (nm)	$E_g^a$ (eV)	$E_{\text{ox}}$ (V)	HOMO <sup>b</sup> (eV)	LUMO <sup>c</sup> (eV)
PA1	705	706	760	1.63	0.85	-5.22	-3.59
PA2	702	702	760	1.63	0.75	-5.12	-3.49
PA3	724	728	780	1.59	0.87	-5.25	-3.66
PA4	754	754	815	1.52	0.55	-4.92	-3.40

<sup>a</sup> Calculated from absorption onset of thin film UV-vis spectra. <sup>b</sup> Determined by cyclic voltammetry from the oxidation potential. <sup>c</sup> Determined from the optical energy band gap and HOMO energy level.

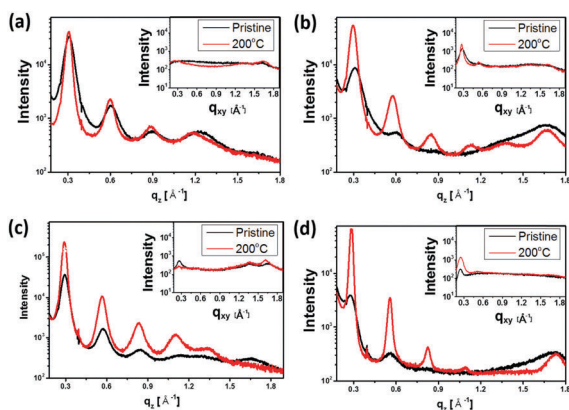


Fig. 2 The XRD patterns of the pristine (black line) and annealed (red line) PA1 film (a) and PA2 film (b), PA3 film (c) and PA4 film (d), respectively. The out of plane and in plane (insets) GIXRD patterns of the four polymers.

polymers exhibited improved molecular ordering with strong ( $h00$ ) diffraction peaks at 0.31, 0.30, 0.29, and 0.28  $\text{\AA}^{-1}$  corresponding to a lamella  $d$ -spacing of 20.6, 21.3, 21.7, and 22.1 nm, respectively. Both phenanthrene-based polymers have slightly shorter  $d$ -spacing than naphthalene-based polymers, which seems to be caused by the wider molecular dimension of phenanthrene. The thermally treated thin films of dimethoxy substituted PA based copolymers, PA2 and PA4, showed arced diffraction in 2D-GIXD patterns (Fig. S10, ESI<sup>†</sup>) and enhanced (010) diffraction corresponding to the  $\pi$ - $\pi$  stacking distance in the  $Q_{xy}$  direction accompanied by ( $h00$ ) diffraction in the  $Q_z$  direction. This indicates that the dimethoxy-substituted polymer chains adopt a mixed edge-on and face-on orientation after thermal treatment. In contrast, the film of unsubstituted PA-based copolymers showed centralized points along the  $Q_z$  axis with an edge-on orientation. From the (010) peaks at 1.66 and 1.64  $\text{\AA}^{-1}$  in the  $Q_{xy}$  direction, the respective  $\pi$ - $\pi$  stacking distance in PA1 and PA3 is about 3.78 nm with a different degree of  $\pi$ - $\pi$  interactions. In addition, the  $\pi$ - $\pi$  stacking distances in a polymer chain with a face-on orientation are 3.76 nm and 3.64 nm for PA2 and PA4, respectively. The shortest  $\pi$ - $\pi$  stacking distance of PA4 is expected to originate from strong intermolecular interactions between the neighboring molecules.

### OFETs and charge transport properties

The charge transport properties of the four (MeO)PA-based copolymers were investigated using top-gate bottom-contact (TGBC) OFETs. For achieving the highest mobility, the film morphology was

optimized by annealing the polymer films at 150, 200, 250, and 300  $^{\circ}\text{C}$  for 30 min at each temperature. The field-effect mobilities of the copolymers were calculated from the saturation regime. The key parameters for OFET performance, the hole mobility ( $\mu_h$ ), the electron mobility ( $\mu_e$ ), and the threshold voltage ( $V_{\text{th}}$ ) are summarized in Table 2. The corresponding transfer and output characteristics of the optimized devices are depicted in Fig. 3 and Fig. S10 (ESI<sup>†</sup>). All copolymers exhibited ambipolar behavior with V-shaped transfer curves with reasonably balanced charge transport properties. The average hole mobilities ( $\mu_{h,\text{ave}}$ ) of pristine PA1, PA2, PA3, and PA4 in the saturation regime are as high as 0.11, 0.09, 0.35 and 0.17  $\text{cm}^2 \text{V}^{-1} \text{s}^{-1}$ , respectively. After thermal annealing, the hole mobilities ( $\mu_{h,\text{ave}}$ ) increased to 0.74, 0.53, 1.10, and 0.62  $\text{cm}^2 \text{V}^{-1} \text{s}^{-1}$  for PA1, PA2, PA3 and PA4, respectively.

This mobility optimization implies that molecular packing became more ordered resulting in a closer  $\pi$ - $\pi$  stacking of the polymer chain, thereby facilitating the charge transport. Furthermore, the average values of optimal electron mobilities ( $\mu_{e,\text{ave}}$ ) have also been increased upon annealing to 0.40, 0.09, 0.90, and 0.17  $\text{cm}^2 \text{V}^{-1} \text{s}^{-1}$  for PA1, PA2, PA3, and PA4, respectively. While the unsubstituted PA-based polymers, PA1 and PA3, exhibited reasonably balanced ambipolar characteristics, dimethoxy substituted PA-based polymers showed hole-dominant ambipolar transport properties accompanied by a larger threshold voltage. This may be caused by a large energy barrier for electron injection due to their higher LUMO energy levels. In addition, both the hole and electron mobilities of PA1 and PA3 that adopt an edge-on orientation of polymer chains are higher than those of PA2 and PA4 with the mixed orientation.

Also, PA2 demonstrated an increase by about 2 orders of magnitude in both hole and electron mobilities compared to those of the polymers with a longer alkoxy side chain on phenanthrene, which were studied previously. It is expected that this improvement in charge transport properties is due to the optimized molecular orientation. PA1 demonstrated further enhanced OFET device performance in the films coated from their trichloroethylene solution with off-center spin coating methods.<sup>53</sup> Annealed PA1 films at 200  $^{\circ}\text{C}$  showed  $\mu_{h,\text{ave}} = 1.27$  and maximum hole mobilities ( $\mu_{h,\text{max}}$ ) up to 1.78  $\text{cm}^2 \text{V}^{-1} \text{s}^{-1}$  (Fig. S12, ESI<sup>†</sup>).<sup>53,54</sup>

### Photovoltaic characteristics

We fabricated BHJ OPV devices to examine the photovoltaic properties of the (MeO)PA-based copolymers as donor materials.

Table 2 OFET characteristics of (MeO)PA based copolymers

Polymer	$T^a$ (°C)	Mobility ( $\text{cm}^2 \text{V}^{-1} \text{S}^{-1}$ )		$V_{\text{th}}$ (V)	
		$\mu_{\text{h,ave(max)}}$	$\mu_{\text{e,ave(max)}}$	$p$	$n$
PA1	None	$1.12 \times 10^{-1}$ ( $1.23 \times 10^{-1}$ )	$4.27 \times 10^{-2}$ ( $5.32 \times 10^{-2}$ )	$-35.2$ ( $\pm 0.84$ )	$64.7$ ( $\pm 1.44$ )
	110	$2.08 \times 10^{-1}$ ( $2.14 \times 10^{-1}$ )	$1.67 \times 10^{-1}$ ( $1.91 \times 10^{-1}$ )	$-37.7$ ( $\pm 1.47$ )	$51.9$ ( $\pm 2.31$ )
	150	$3.51 \times 10^{-1}$ ( $4.20 \times 10^{-1}$ )	$2.60 \times 10^{-1}$ ( $3.00 \times 10^{-1}$ )	$-39.0$ ( $\pm 1.85$ )	$57.7$ ( $\pm 2.31$ )
	200	$7.43 \times 10^{-1}$ ( $9.30 \times 10^{-1}$ )	$3.97 \times 10^{-1}$ ( $5.47 \times 10^{-1}$ )	$-42.2$ ( $\pm 1.92$ )	$56.8$ ( $\pm 0.93$ )
	250	$4.55 \times 10^{-1}$ ( $5.67 \times 10^{-1}$ )	$2.76 \times 10^{-1}$ ( $3.22 \times 10^{-1}$ )	$-43.3$ ( $\pm 2.03$ )	$57.3$ ( $\pm 0.86$ )
PA2	None	$9.31 \times 10^{-2}$ ( $1.37 \times 10^{-1}$ )	$1.58 \times 10^{-2}$ ( $2.03 \times 10^{-2}$ )	$-36.9$ ( $\pm 3.12$ )	$63.9$ ( $\pm 1.92$ )
	110	$2.12 \times 10^{-1}$ ( $2.98 \times 10^{-1}$ )	$3.22 \times 10^{-2}$ ( $4.33 \times 10^{-2}$ )	$-45.8$ ( $\pm 2.69$ )	$61.9$ ( $\pm 0.76$ )
	150	$3.31 \times 10^{-1}$ ( $4.39 \times 10^{-1}$ )	$4.06 \times 10^{-2}$ ( $4.80 \times 10^{-2}$ )	$-55.3$ ( $\pm 2.12$ )	$62.6$ ( $\pm 2.26$ )
	200	$5.31 \times 10^{-1}$ ( $6.61 \times 10^{-1}$ )	$9.42 \times 10^{-2}$ ( $1.28 \times 10^{-1}$ )	$-52.3$ ( $\pm 2.52$ )	$66.4$ ( $\pm 0.83$ )
	250	$4.61 \times 10^{-1}$ ( $5.35 \times 10^{-1}$ )	$7.32 \times 10^{-2}$ ( $1.01 \times 10^{-1}$ )	$-54.2$ ( $\pm 1.94$ )	$66.9$ ( $\pm 1.95$ )
PA3	None	$3.50 \times 10^{-1}$ ( $4.17 \times 10^{-1}$ )	$2.81 \times 10^{-1}$ ( $3.27 \times 10^{-1}$ )	$-33.5$ ( $\pm 2.54$ )	$49.87$ ( $\pm 0.64$ )
	110	$4.13 \times 10^{-1}$ ( $4.92 \times 10^{-1}$ )	$2.14 \times 10^{-1}$ ( $2.27 \times 10^{-1}$ )	$-44.9$ ( $\pm 1.43$ )	$50.1$ ( $\pm 1.41$ )
	150	$4.84 \times 10^{-1}$ ( $5.65 \times 10^{-1}$ )	$5.61 \times 10^{-1}$ ( $5.95 \times 10^{-1}$ )	$-38.3$ ( $\pm 1.32$ )	$52.2$ ( $\pm 2.05$ )
	200	$5.06 \times 10^{-1}$ ( $6.22 \times 10^{-1}$ )	$4.79 \times 10^{-1}$ ( $5.87 \times 10^{-1}$ )	$-43.7$ ( $\pm 1.24$ )	$52.2$ ( $\pm 1.26$ )
	250	$1.10$ (1.30)	$9.00 \times 10^{-1}$ (1.38)	$-47.0$ ( $\pm 2.10$ )	$50.7$ ( $\pm 1.27$ )
300	$4.97 \times 10^{-1}$ ( $6.02 \times 10^{-1}$ )	$4.55 \times 10^{-1}$ ( $5.12 \times 10^{-1}$ )	$-44.2$ ( $\pm 1.51$ )	$47.8$ ( $\pm 2.54$ )	
PA4	None	$1.68 \times 10^{-1}$ ( $2.13 \times 10^{-1}$ )	$1.55 \times 10^{-2}$ ( $2.13 \times 10^{-2}$ )	$-34.6$ ( $\pm 1.56$ )	$62.16$ ( $\pm 1.79$ )
	100	$1.92 \times 10^{-1}$ ( $2.08 \times 10^{-1}$ )	$2.80 \times 10^{-2}$ ( $3.17 \times 10^{-2}$ )	$-35.6$ ( $\pm 0.96$ )	$61.8$ ( $\pm 2.54$ )
	150	$6.19 \times 10^{-1}$ ( $7.11 \times 10^{-1}$ )	$1.33 \times 10^{-1}$ ( $1.45 \times 10^{-1}$ )	$-44.3$ ( $\pm 2.03$ )	$60.7$ ( $\pm 0.76$ )
	200	$5.36 \times 10^{-1}$ ( $6.99 \times 10^{-1}$ )	$1.66 \times 10^{-1}$ ( $1.87 \times 10^{-1}$ )	$-42.7$ ( $\pm 1.74$ )	$57.3$ ( $\pm 1.25$ )
	250	$3.02 \times 10^{-1}$ ( $3.80 \times 10^{-1}$ )	$1.35 \times 10^{-1}$ ( $1.48 \times 10^{-1}$ )	$-49.0$ ( $\pm 0.52$ )	$54.5$ ( $\pm 1.03$ )

<sup>a</sup> Annealing temperature.

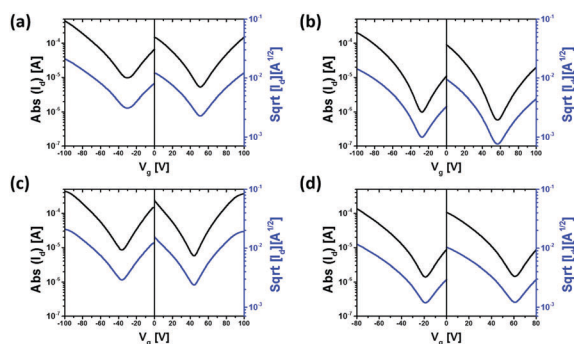


Fig. 3 Transfer characteristics of OFET devices of (MeO)PA-based polymer films after annealing: (a) PA1 at 200 °C, (b) PA2 at 200 °C, (c) PA3 at 250 °C and (d) PA4 at 150 °C.

The inverted device structure of indium tin oxide (ITO)/ITO/ZnO/polymer:PC<sub>71</sub>BM/MoO<sub>3</sub>/Ag was employed under the illumination of AM 1.5G at 100 mW cm<sup>-2</sup>. The PCEs and all key parameters of the optimized devices for each polymer are summarized in Table 3 and representative current density–voltage ( $J$ – $V$ ) characteristics are shown in Fig. 4a. As already mentioned, all copolymers showed the

best solubility in chloroform. However, chloroform is difficult to handle due to its low boiling point. To achieve good processability and nanoscale phase separation of polymer:PC<sub>71</sub>BM, we use 3% v/v of diphenyl ether (DPE) with a high boiling point as a processing additive. The optimized devices were made with a weight ratio of 1 : 3 for each polymer:PC<sub>71</sub>BM and the best device exhibited a PCE of 5.3, 4.8, 5.8, and 4.1% for PA1, PA2, PA3 and PA4, respectively. The PA1-based devices had a PCE of 5.3%, a  $J_{\text{sc}}$  of 11.5 mA cm<sup>-2</sup>, a FF of 63%, and a  $V_{\text{oc}}$  of 0.72 V. The PA2 based device exhibited a similar  $J_{\text{sc}}$  (12.2 mA cm<sup>-2</sup>) and FF (0.68) but slightly lower PCE (4.8%) than PA1 because of the lower  $V_{\text{oc}}$  (0.68 V) due to its higher HOMO energy level. Upon replacing the longer alkoxy side chain on phenanthrene with the shortest methoxy group, PA2:PC<sub>71</sub>BM based OPVs exhibited enhanced device performance especially in terms of  $J_{\text{sc}}$ , compared to PA3 and PA4 in our previous work. There could be several reasons for this improvement. PA2 showed better charge transport properties than previous materials, and the PA2:PC<sub>71</sub>BM blend film exhibited much finer phase separation between the donor and acceptor for efficient exciton dissociation. In addition, the use of PC<sub>71</sub>BM instead of PC<sub>61</sub>BM led to stronger photon absorption in the shorter wavelength region.

Table 3 Photovoltaic characteristics of optimized devices

Polymer <sup>a</sup>	$J_{\text{sc}}^b$ (mA cm <sup>-2</sup> )	$V_{\text{oc}}$ (V)	FF (%)	PCE (%)	$d^c$ (nm)	$J_{\text{sc}}^d$ (mA cm <sup>-2</sup> )
PA1	11.5	0.72	63	5.3	100	11.9
PA2	12.2	0.68	57	4.8	120	11.6
PA3	12.6	0.75	61	5.8	120	12.0
PA4	12.5	0.57	58	4.1	100	12.2

<sup>a</sup> Polymer:PC<sub>71</sub>BM (1 : 3, w/w). <sup>b</sup> Short circuit current from the  $J$ – $V$  curve. <sup>c</sup> Thickness of the active layer. <sup>d</sup> Determined by integrating the EQE spectrum with the AM 1.5G spectrum.

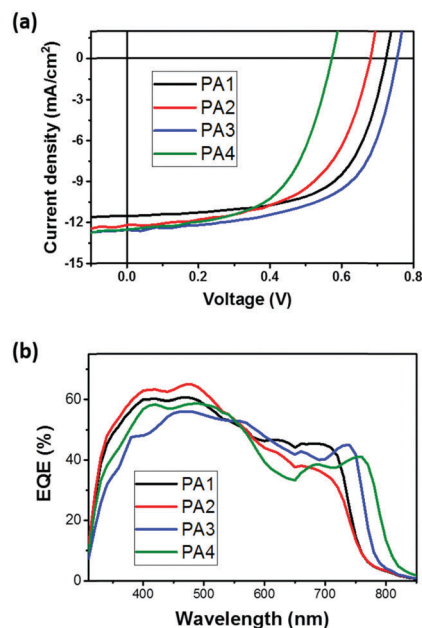


Fig. 4 (a) Current density–voltage ( $J$ – $V$ ) curves of OPV devices with the structure of ITO/ZnO/polymer:PC<sub>71</sub>BM/MoO<sub>3</sub>/Ag under AM 1.5G illumination (100 mW cm<sup>-2</sup>). (b) EQE curves of the corresponding OPV devices.

While **PA3** showed the highest PCE of 5.8% with a  $J_{sc}$  of 12.6 mA cm<sup>-2</sup>, a FF of 61%, and a  $V_{oc}$  of 0.75 V, the PCE of **PA4** was only 4% with the lowest  $V_{oc}$  (0.57 V) in accordance with the position of the HOMO energy level. In BHJ OPVs,  $V_{oc}$  is determined as

$$V_{oc} = \frac{1}{e} (E_{LUMO}^{acceptor} - E_{HOMO}^{donor} - \Delta) - \frac{kT}{e} \ln \left( \frac{n_e n_h}{N_c^2} \right)$$

Here,  $E_{LUMO}^{acceptor}$  is the LUMO energy level of the acceptor;  $E_{HOMO}^{donor}$  is the HOMO energy level of the donor polymer;  $n_e$  and  $n_h$  are the electron and hole densities in the acceptor and donor polymer domains at open circuit, respectively; and  $N_c$  is the effective density of states.<sup>55,56</sup> The  $V_{oc}$  value is directly related to the energy difference between the HOMO level of the donor polymers and the LUMO energy level of PC<sub>71</sub>BM.<sup>19</sup> Thus, the OPV devices based on **PA4** had the lowest  $V_{oc}$  values because **PA4** has the highest HOMO energy level. The optimized device of each polymer showed a large difference in the  $V_{oc}$  value which is consistent with the HOMO energy level of polymers rather than the photocurrent or FF.

External quantum efficiencies (EQEs) were measured for each OPV under optimized device conditions in order to evaluate the photoresponse of (MeO)PA-copolymers and calibrate the  $J_{sc}$  value (Fig. 4b). The  $J_{sc}$  values derived from integrating the EQE curves are within 5% error compared to the respective  $J_{sc}$  obtained from the  $J$ – $V$  curve. All devices show a broad spectral response from the 300 nm to near 800 nm region. The EQE plots of the (MeO)PA polymer based devices yielded similar results to the absorption spectra of the polymers in the long wavelength region and the PCBM absorption spectra in the short wavelength region. This indicates that excitons were generated in both PCBM

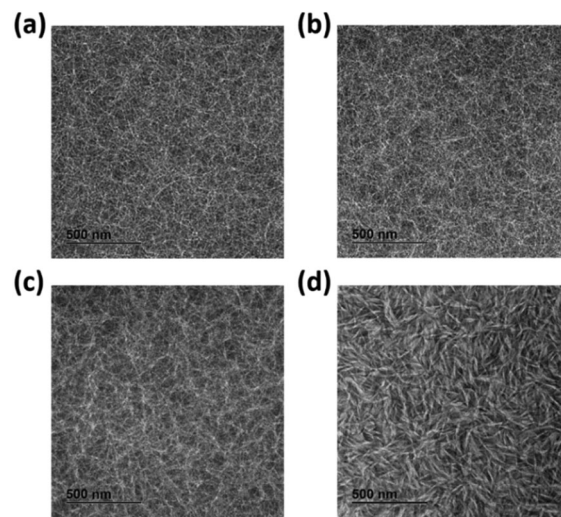


Fig. 5 TEM images of (a) **PA1**:PC<sub>71</sub>BM (1:3, w/w), (b) **PA2**:PC<sub>71</sub>BM (1:3, w/w), (c) **PA3**:PC<sub>71</sub>BM (1:3, w/w) and (d) **PA4**:PC<sub>71</sub>BM (1:3, w/w), respectively.

and the polymer phase. **PA2** based devices exhibited a maximum EQE of 65% at 475 nm but lowest EQE in the polymer region. The overall  $J_{sc}$  values integrated from EQE curves are quite similar to other polymers.

The photoactive layer morphology of the optimized devices was observed using transmission electron microscopy (TEM), as shown in Fig. 5. The film morphologies of phenanthrene-based copolymers (**PA1** and **PA2**):PC<sub>71</sub>BM show finer dispersed fibrils with an interpenetrating bicontinuous network that facilitates efficient exciton dissociation, which is directly related to photocurrent generation.<sup>22,57,58</sup> Also, **PA3**:PC<sub>71</sub>BM films exhibited a similar morphology to phenanthrene-based polymers but slightly coarser. In contrast, **PA4**:PC<sub>71</sub>BM films displayed fibrillar polymer aggregation and a large domain size of over 20 nm, which is considered to be close to the limit of exciton diffusion length, due to limited solubility of **PA4**. Thus, despite the lowest optical band gap of **PA4**, the photocurrent is reasonably similar to that of other copolymers.

The light intensity dependencies of  $J_{sc}$  and  $V_{oc}$  were observed by examining the charge recombination characteristics using a filter with different densities. Fig. S13a (ESI<sup>†</sup>) shows a log–log plot of the corresponding  $J_{sc}$  as a function of light intensity ( $I$ ). Because the generation rate of electron and hole pairs is related to photon absorption, the photocurrent is expected to be proportional to the light intensity. From a power law dependence of  $J_{sc}$  upon  $I$  ( $J_{sc} \propto I^\alpha$ , where  $\alpha$  is typically from 0.85 to 1), when  $\alpha$  is close to 1, carrier loss induced by bimolecular recombination between mobile electrons and holes at the interface of the donor/acceptor heterojunction is reduced.<sup>10,55,56,59–61</sup> Although all (MeO)PA-based copolymers showed  $\alpha$  close to 1, phenanthrene based copolymers had slightly lower  $\alpha$  values (0.978 for **PA1** and 0.977 for **PA2**) than naphthalene based copolymers (0.992 for both **PA3** and **PA4**), which indicates that the bimolecular recombination strength is slightly higher in the device composed of phenanthrene based copolymers. In addition, Fig. S13b (ESI<sup>†</sup>) shows the dependence of the  $V_{oc}$  on light intensity for the

optimized devices with each of the (MeO)PA-based copolymers. When Shockley–Read–Hall (SRH) recombination, also called trap-assisted recombination, is dominant, the slope of  $\delta V_{oc}$  versus  $\ln(I)$  increases from  $kT/e$  (bimolecular recombination only) to  $2kT/e$ , where  $k$  is the Boltzmann constant,  $T$  is the absolute temperature, and  $e$  is the electron charge.<sup>62–64</sup> The OPVs processed with (MeO)PA-based copolymers exhibited a slope in the range from  $1.12kT/e$  to  $1.18kT/e$ . Therefore, both geminate recombination and non-geminate recombination coexist, though bimolecular recombination dominates.

## Conclusion

Four kinds of D–A type copolymers based on polyaromatic compounds were synthesized *via* Suzuki polymerization for OFETs and OPVs. All (MeO)PA-based copolymers exhibited small band gap properties ( $E_g = 1.63$ – $1.52$  eV) due to their weak donor–strong acceptor structural strategies. Dimethoxy substituents affected the absorption spectra and energy levels slightly differently depending on the polyaromatic units. As expected, dimethoxy substituents elevated the HOMO and LUMO energy levels, and especially, the energy level of the naphthalene-based copolymer was highly affected compared to those of the phenanthrene-based copolymers. **PA4** containing 1,5-dimethoxynaphthalene had the smallest energy band gap (1.52 eV) and the highest HOMO level ( $-4.92$  eV) among the copolymers. The electron density of **PA4** is highly increased through dimethoxy substituents at opposite sides of the naphthalene unit. The HOMO distribution of 1,5-dimethoxynaphthalene is a well-delocalized conjugated system while 9,10-dimethoxyphenanthrene showed similar distribution with unsubstituted phenanthrene. In the case of phenanthrene, the electron-donating mesomeric effect of one methoxy group is relatively decreased due to the electron-withdrawing inductive effect of the methoxy-oxygen which is substituted close to the mesomeric methoxy group. With their relatively higher HOMO levels, the MeOPA based polymers, **PA2** and **PA4**, showed a hole-dominant ambipolar charge transport and **PA1** and **PA3**, without dimethoxy substituents, exhibited reasonably balanced ambipolar charge-transport characteristics with hole and electron mobilities of  $\sim 1 \text{ cm}^2 \text{ V}^{-1} \text{ s}^{-1}$ . The **PA1**-based OFET casted from TCE solution using an off-center spin-coating method exhibited the best field-effect performance with a maximum hole mobility ( $\mu_{h,max}$ ) of  $1.77 \text{ cm}^2 \text{ V}^{-1} \text{ s}^{-1}$ . The inverted OPV devices fabricated using (MeO)PA based copolymer:PC<sub>71</sub>BM blends exhibited PCEs of 5.3%, 4.8%, 5.8%, and 4.1% for **PA1**, **PA2**, **PA3**, and **PA4**, respectively. However, dimethoxy substituents on polyaromatic compounds had a negative effect on  $V_{oc}$  in particular and a slight influence on  $J_{sc}$  or FF.

## Experimental

### Characterization

<sup>1</sup>H NMR spectra were recorded using a JEOL JNM-ECX400 spectrometer using CDCl<sub>3</sub> as a solvent. Gel permeation chromatography

(GPC) was performed on an Acme 9000 using 1,2,4-trichlorobenzene as an eluent at 150 °C and calibrated with polystyrene standards. The optimized geometry of isolated polymer repeating units were calculated using the DFT calculation based on the B3LYP/6-311G(d,p) basis set using the GAUSSIAN 09 program. UV-vis absorption spectra and time-dependent UV-vis absorption spectra were recorded using a Lambda 750 (Perkin-Elmer) spectrometer and VARIAN-5000 spectrophotometer, respectively. Cyclic voltammetry was performed on a potentiostat (Eco Chemie AUTOLAB) with an electrolyte solution of 0.1 M tetrabutylammonium perchlorate in acetonitrile at a scan rate of 100 mV s<sup>-1</sup>. Ag/Ag<sup>+</sup>, Pt wire, and polymer coated ITO substrates were used as a reference, a counter, and a working electrode, respectively. The atomic force microscopy (AFM) images were obtained using a Veeco AFM microscope in tapping mode under ambient conditions and transmission electron microscopy (TEM) was performed using a Tecnai G2 S-Twin 3600 keV electron microscope. GIWAXD of polymer thin films on a Si/SiO<sub>2</sub> wafer was performed using the beamline 9A with an incident energy of 11.57 keV at the Pohang Accelerator Laboratory.

### Synthesis of monomers

2,7-Dibromophenanthrene and 2,7-dibromo-9,10-dimethoxyphenanthrene were synthesized following the procedures described in the literature.<sup>44–47</sup> 2,6-Dibromonaphthalene was purchased from TCI chemical and used without further purification.

**2,7-Bis(4,4,5,5-tetramethyl-1,3,2-dioxaborolan-2-yl)phenanthrene (MO1)**. To a solution of 2,7-dibromophenanthrene (1.00 g, 3 mmol), bis(pinacolato)diboron (1.82 g, 7.2 mmol) and potassium acetate (1.47 g, 15 mmol) in anhydrous dioxane (50 ml) was added Pd(dppp)Cl<sub>2</sub> (0.05 g, 0.06 mmol), and the reaction mixture was heated to reflux for 72 h under a nitrogen atmosphere. After cooling down to room temperature, the reaction mixture was extracted with chloroform and stirred with Celite and activated carbon for 1 hour. After this, the solvent was removed and the residue was purified by column chromatography on a silica gel with chloroform as an eluent. The solution was condensed and a solid compound was recrystallized in methanol. The product was afforded as white crystals (1.08 g, yield 84%). <sup>1</sup>H NMR (400 MHz, CDCl<sub>3</sub>, ppm): 8.69 (d, 2H), 8.38 (s, 2H), 8.04 (d, 2H), 7.76 (s, 2H), 1.40 (s, 24H).

**2,2'-(9,10-Dimethoxyphenanthrene-2,7-diyl)bis(4,4,5,5-tetramethyl-1,3,2-dioxaborolane) (MO2)**. **MO2** was prepared following the same procedure as for **MO1**. The product was afforded as white crystals (1.3 g, yield 89%). <sup>1</sup>H NMR (400 MHz, CDCl<sub>3</sub>, ppm): 8.71 (s, 2H), 8.64 (d, 2H), 7.99 (d, 2H), 4.11 (s, 6H), 1.40 (s, 24H).

**2,6-Bis(4,4,5,5-tetramethyl-1,3,2-dioxaborolan-2-yl)naphthalene (MO3)**. **MO3** was prepared following the same procedure as for **MO1**. The product was afforded as white crystals (1.19 g, yield 91%). <sup>1</sup>H NMR (400 MHz, CDCl<sub>3</sub>, ppm): 8.35 (s, 2H), 7.84 (q, 4H), 1.39 (s, 24H).

**2,2'-(4,8-Dimethoxynaphthalene-2,6-diyl)bis(4,4,5,5-tetramethyl-1,3,2-dioxaborolane) (MO4)**. To a solution of 1,5-dimethoxynaphthalene (1.88 g, 10 mmol), pinacolborane (3.20 g, 25 mmol), and 4,4'-di-*tert*-butyl-2,2'-bipyridine (0.02 g, 0.1 mmol) in anhydrous THF (50 ml) was added [Ir(COD)OMe]<sub>2</sub> (0.02 g, 2.5 μmol),

and the reaction mixture was heated to reflux for 48 h under a nitrogen atmosphere. After cooling down to room temperature, the reaction mixture was extracted with chloroform and stirred with Celite, and then the residue was purified by column chromatography on a silica gel with chloroform:hexane (1:1) as an eluent. The product was afforded as white crystals (1.32 g, yield 31%).  $^1\text{H NMR}$  (400 MHz,  $\text{CDCl}_3$ , ppm): 8.37 (s, 2H), 7.18 (s, 2H), 4.03 (s, 2H), 1.38 (s, 24H).

3,6-Bis(5-bromothiophen-2-yl)-2,5-bis(2-decyltetradecyl)-2,5-dihydropyrrolo[3,4-*c*]pyrrole-1,4-dione (**DTDPP**).  $^1\text{H NMR}$  (400 MHz,  $\text{CDCl}_3$ , ppm): 8.63 (d, 2H), 7.22 (d, 2H), 3.92 (d, 4H), 1.92-1.82 (m, 2H), 1.38-1.12 (m, 48H), 0.87 (t, 12H).

### General procedures for polymerization

(MeO)PA-DPP alternating copolymers were synthesized *via* Suzuki polymerization with the same procedure as that followed in the literature.<sup>65</sup> 0.4 mmol of each comonomer and reactant was refluxed for 3 days, then 0.1 mg of phenyl boronic acid and 1 ml of bromobenzene were added as end-cappers for an additional 12 hours each. After cooling down to room temperature, the reaction mixture was poured into methanol containing 20 v/v% hydrochloric acid and stirred for 3 hours. The solid compound was filtered and then purified *via* Soxhlet extraction with methanol, acetone, hexane and chloroform. The chloroform solution fraction was concentrated and precipitated into methanol. The solid was filtered and dried in a vacuum oven for 12 hours at 70 °C.

Poly{phenanthrene-2,7-diyl-*alt*-3,6-dithiophene-2-yl-2,5-di(2-decyltetradecyl)-pyrrolo[3,4-*c*]pyrrole-1,4-dione} (**PA1**) (401 mg, yield: 87.2%). Anal. calcd for  $(\text{C}_{76}\text{H}_{110}\text{N}_2\text{O}_2\text{S}_2)_n$ : C, 79.51; H, 9.68; N, 2.44; O, 2.79; S, 5.58. Found: C, 78.28; H, 9.83; N, 2.54; O, 2.91; S, 5.32.  $M_n = 54.2 \text{ kg mol}^{-1}$ ,  $M_w = 175 \text{ kg mol}^{-1}$ , PDI = 3.23.

Poly{9,10-dimethoxyphenanthrene-2,7-diyl-*alt*-3,6-dithiophene-2-yl-2,5-di(2-decyltetradecyl)-pyrrolo[3,4-*c*]pyrrole-1,4-dione} (**PA2**) (361 mg, yield: 74.6%). Anal. calcd for  $(\text{C}_{78}\text{H}_{114}\text{N}_2\text{O}_4\text{S}_2)_n$ : C, 77.54; H, 9.53; N, 2.32; O, 5.30; S, 5.31. Found: C, 76.21; H, 9.69; N, 2.41; O, 5.67; S, 5.19.  $M_n = 66.5 \text{ kg mol}^{-1}$ ,  $M_w = 135 \text{ kg mol}^{-1}$ , PDI = 2.03.

Poly{naphthalene-2,6-diyl-*alt*-3,6-dithiophene-2-yl-2,5-di(2-decyltetradecyl)-pyrrolo[3,4-*c*]pyrrole-1,4-dione} (**PA3**) (386 mg, yield: 87.6%). Anal. calcd for  $(\text{C}_{72}\text{H}_{108}\text{N}_2\text{O}_2\text{S}_2)_n$ : C, 78.76; H, 9.94; N, 2.55; O, 2.91; S, 5.84. Found: C, 79.00; H, 9.73; N, 2.72; O, 3.09; S, 5.49.  $M_n = 56.8 \text{ kg mol}^{-1}$ ,  $M_w = 105 \text{ kg mol}^{-1}$ , PDI = 1.84.

Poly{1,5-dimethoxynaphthalene-3,7-diyl-*alt*-3,6-dithiophene-2-yl-2,5-di(2-decyltetradecyl)-pyrrolo[3,4-*c*]pyrrole-1,4-dione} (**PA4**) (392 mg, yield: 84.3%). Anal. calcd for  $(\text{C}_{74}\text{H}_{112}\text{N}_2\text{O}_4\text{S}_2)_n$ : C, 76.75; H, 9.77; N, 2.42; O, 5.53; S, 5.54. Found: C, 77.02; H, 9.61; N, 2.24; O, 5.81; S, 5.41.  $M_n = 23.4 \text{ kg mol}^{-1}$ ,  $M_w = 48.9 \text{ kg mol}^{-1}$ , PDI = 2.09.

### Fabrication of OFET devices

OFETs were fabricated using a top-gate/bottom-contact configuration with a 20  $\mu\text{m}$  channel length ( $L$ ) and 1 mm width ( $W$ ). The source and drain electrodes are patterned onto a glass substrate with the evaporation of gold/nickel (14 nm/4 nm thick).

The substrates were cleaned using acetone, DI water, and isopropanol for 10 min each in an ultrasonicator, and dried in an oven. Before polymer deposition, the substrates were UV-ozone treated for 20 min. Each polymer was dissolved in a cosolvent composed of chloroform:*o*-dichlorobenzene (4:1, v/v%) with a concentration of 3.5  $\text{mg ml}^{-1}$ . The polymer solution was spin-coated onto a substrate under a nitrogen atmosphere. The polymer films were thermally annealed at 150, 200, 250, and 300 °C for 30 min. Then, PMMA (80  $\text{mg ml}^{-1}$  in *n*-butyl acetate) was deposited as a gate dielectric layer and annealed at 80 °C for 2 hours in the nitrogen-filled glove box. The gate electrode was thermally evaporated with aluminium through a shadow mask. The electrical characteristics of individual OFET devices were measured using a Keithley 4200-SCS under a nitrogen atmosphere.

### Fabrication of OPV devices

OPVs were fabricated with an inverted configuration of ITO/ZnO/active layer/MoO<sub>3</sub>/Ag in order to evaluate the photovoltaic properties of the polymers. ITO-patterned glass substrates were cleaned using acetone, DI water, and isopropanol for 10 min each in an ultrasonicator, and dried in an oven. Before polymer deposition, the substrates were UV-ozone treated for 20 min. The zinc oxide (ZnO) layer was deposited using ZnO nanoparticle dispersion in isopropanol (2.5 wt%), then baked at 120 °C for 10 min. Then the substrates were transferred into a nitrogen-filled glove box. The photoactive layer was spin-coated using each polymer:PC<sub>71</sub>BM solution which was dissolved in chloroform containing 3 v/v% of diphenyl ether (DPE) and stirred for 2 hours. Then, molybdenum oxide and silver electrodes were thermally evaporated with a thickness of 10 nm and 100 nm, respectively. The photovoltaic characteristics were measured using a Keithley 4200 under the illumination of AM 1.5G at 100  $\text{mW cm}^{-2}$ .

## Conflicts of interest

There are no conflicts to declare.

## Acknowledgements

This work was supported by the National Research Foundation of Korea (NRF) grant funded by the Korea government (NRF-2015R1A2A1A10054466), the Korea Institute of Energy Technology Evaluation and Planning (KETEP) and the Ministry of Trade, Industry & Energy (MOTIE) of the Republic of Korea (No. 20153010012110), and the GIST Research Institute (GRI) grant funded by the GIST in 2017. The GIXD was measured using the synchrotron radiation source 9A beamline at the Pohang Accelerator Laboratory (PAL).

## References

- H. Yan, Z. Chen, Y. Zheng, C. Newman, J. R. Quinn, F. Dötz, M. Kastler and A. Facchetti, *Nature*, 2009, **457**, 679–686.
- J. S. Yeo, J. M. Yun, D. Y. Kim, S. S. Kim and S. I. Na, *Sol. Energy Mater. Sol. Cells*, 2013, **114**, 104–109.

- 3 S. Günes, H. Neugebauer and N. S. Sariciftci, *Chem. Rev.*, 2007, **107**, 1324–1338.
- 4 Y. Li, K. Yao, H. L. Yip, F. Z. Ding, Y. X. Xu, X. Li, Y. Chen and A. K. Y. Jen, *Adv. Funct. Mater.*, 2014, **24**, 3631–3638.
- 5 P. S. K. Amegadze and Y.-Y. Noh, *J. Inf. Disp.*, 2014, **15**, 213–229.
- 6 D. Khim, H. Han, K. J. Baeg, J. Kim, S. W. Kwak, D. Y. Kim and Y. Y. Noh, *Adv. Mater.*, 2013, **25**, 4302–4308.
- 7 K. J. Baeg, D. Khim, J. Kim, D. Y. Kim, S. W. Sung, B. Do Yang and Y. Y. Noh, *IEEE Electron Device Lett.*, 2013, **34**, 126–128.
- 8 H. A. M. Van Mullekom, J. A. J. M. Vekemans, E. E. Havinga and E. W. Meijer, *Developments in the chemistry and band gap engineering of donor-acceptor substituted conjugated polymers*, 2001, vol. 32.
- 9 S. Yum, T. K. An, X. Wang, W. Lee, M. A. Uddin, Y. J. Kim, T. L. Nguyen, S. Xu, S. Hwang, C. E. Park and H. Y. Woo, *Chem. Mater.*, 2014, **26**, 2147–2154.
- 10 M. A. Uddin, T. H. Lee, S. Xu, S. Y. Park, T. Kim, S. Song, T. L. Nguyen, S. J. Ko, S. Hwang, J. Y. Kim and H. Y. Woo, *Chem. Mater.*, 2015, **27**, 5997–6007.
- 11 A. Facchetti, *Chem. Mater.*, 2011, **23**, 733–758.
- 12 G. Horowitz, *Adv. Mater.*, 1998, **10**, 365–377.
- 13 W. Zhang, Y. Han, X. Zhu, Z. Fei, Y. Feng, N. D. Treat, H. Faber, N. Stingelin, I. McCulloch, T. D. Anthopoulos and M. Heaney, *Adv. Mater.*, 2016, **28**, 3922–3927.
- 14 P. Boufflet, Y. Han, Z. Fei, N. D. Treat, R. Li, D. M. Smilgies, N. Stingelin, T. D. Anthopoulos and M. Heaney, *Adv. Funct. Mater.*, 2015, **25**, 7038–7048.
- 15 W. Lee, G. H. Kim, S. J. Ko, S. Yum, S. Hwang, S. Cho, Y. H. Shin, J. Y. Kim and H. Y. Woo, *Macromolecules*, 2014, **47**, 1604–1612.
- 16 A. Casey, Y. Han, Z. Fei, A. J. P. White, T. D. Anthopoulos and M. Heaney, *J. Mater. Chem. C*, 2015, **3**, 265–275.
- 17 R. Kroon, M. Lenes, J. C. Hummelen, P. W. M. Blom and B. de Boer, *Small Bandgap Polymers for Organic Solar Cells (Polymer Material Development in the Last 5 Years)*, 2008, vol. 48.
- 18 A. Facchetti, *Mater. Today*, 2013, **16**, 123–132.
- 19 C. J. Brabec, A. Cravino, D. Meissner, N. Serdar Sariciftci, T. Fromherz, M. T. Rispens, L. Sanchez and J. C. Hummelen, *Adv. Funct. Mater.*, 2001, **11**, 374–380.
- 20 A. Gadisa, M. Svensson, M. R. Andersson and O. Inganäs, *Appl. Phys. Lett.*, 2004, **84**, 1609–1611.
- 21 M. C. Scharber, D. Mühlbacher, M. Koppe, P. Denk, C. Waldauf, A. J. Heeger and C. J. Brabec, *Adv. Mater.*, 2006, **18**, 789–794.
- 22 Y. Huang, E. J. Kramer, A. J. Heeger and G. C. Bazan, *Chem. Rev.*, 2014, **114**, 7006–7043.
- 23 C. A. Junwu and C. Yong, *Acc. Chem. Res.*, 2009, **42**, 1709–1718.
- 24 A. Casey, S. D. Dimitrov, P. Shakya-Tuladhar, Z. Fei, M. Nguyen, Y. Han, T. D. Anthopoulos, J. R. Durrant and M. Heaney, *Chem. Mater.*, 2016, **28**, 5110–5120.
- 25 D. Gupta, S. Mukhopadhyay and K. S. Narayan, *Sol. Energy Mater. Sol. Cells*, 2010, **94**, 1309–1313.
- 26 Z. Wu, A. Li, B. Fan, F. Xue, C. Adachi and J. Ouyang, *Sol. Energy Mater. Sol. Cells*, 2011, **95**, 2516–2523.
- 27 S. Xiao, A. C. Stuart, S. Liu, H. Zhou and W. You, *Adv. Funct. Mater.*, 2010, **20**, 635–643.
- 28 J. D. Yuen, J. Fan, J. Seiffter, B. Lim, R. Hufschmid, A. J. Heeger and F. Wudl, *J. Am. Chem. Soc.*, 2011, **133**, 20799–20807.
- 29 S. Qu and H. Tian, *Chem. Commun.*, 2012, **48**, 3039.
- 30 Y. Huang, F. Liu, X. Guo, W. Zhang, Y. Gu, J. Zhang, C. C. Han, T. P. Russell and J. Hou, *Adv. Energy Mater.*, 2013, **3**, 930–937.
- 31 C. Kanimozhi, P. Balraju, G. D. Sharma and S. Patil, *J. Phys. Chem. B*, 2010, **114**, 3095–3103.
- 32 E. Zhou, S. Yamakawa, K. Tajima, C. Yang and K. Hashimoto, *Chem. Mater.*, 2009, **21**, 4055–4061.
- 33 W. Li, K. H. Hendriks, M. M. Wienk and R. A. J. Janssen, *Acc. Chem. Res.*, 2016, **49**, 78–85.
- 34 Y.-A. Kim, K.-I. Hwang, M. Kang, N.-K. Kim, S. Jang, I.-B. Kim, J. Kim and D.-Y. Kim, *Org. Electron.*, 2017, **44**, 238–246.
- 35 H. Tian, J. Shi, S. Dong, D. Yan, L. Wang, Y. Geng and F. Wang, *Chem. Commun.*, 2006, 3498–3500.
- 36 M. Y. Jo, J. H. Bae, G. E. Lim, Y. E. Ha, H. E. Katz and J. H. Kim, *Synth. Met.*, 2013, **176**, 41–46.
- 37 M. Shahid, R. S. Ashraf, Z. Huang, A. J. Kronemeijer, T. McCarthy-Ward, I. McCulloch, J. R. Durrant, H. Sirringhaus and M. Heaney, *J. Mater. Chem.*, 2012, **22**, 12817.
- 38 L. Huo, J. Hou, H. Y. Chen, S. Zhang, Y. Jiang, T. L. Chen and Y. Yang, *Macromolecules*, 2009, **42**, 6564–6571.
- 39 R. S. Ashraf, I. Meager, M. Nikolka, M. Kirkus, M. Planells, B. C. Schroeder, S. Holliday, M. Hurhangee, C. B. Nielsen, H. Sirringhaus and I. McCulloch, *J. Am. Chem. Soc.*, 2015, **137**, 1314–1321.
- 40 J. S. Lee, S. K. Son, S. Song, H. Kim, D. R. Lee, K. Kim, M. J. Ko, D. H. Choi, B. S. Kim and J. H. Cho, *Chem. Mater.*, 2012, **24**, 1316–1323.
- 41 J. Gao, L. Dou, W. Chen, C.-C. Chen, X. Guo, J. You, B. Bob, W.-H. Chang, J. Strzalka, C. Wang, G. Li and Y. Yang, *Adv. Energy Mater.*, 2014, **4**, 130079.
- 42 J. R. Matthews, W. Niu, A. Tandia, A. L. Wallace, J. Hu, W. Y. Lee, G. Giri, S. C. B. Mannsfeld, Y. Xie, S. Cai, H. H. Fong, Z. Bao and M. He, *Chem. Mater.*, 2013, **25**, 782–789.
- 43 P. Sonar, T. R. B. Foong and A. Dodabalapur, *Phys. Chem. Chem. Phys.*, 2014, **16**, 4275–4283.
- 44 Y. Qin, *Polym. Int.*, 2008, **57**, 171–180.
- 45 B. N. Boden, K. J. Jardine, A. C. W. Leung and M. J. MacLachlan, *Org. Lett.*, 2006, **8**, 1855–1858.
- 46 J. W. Ciszek and J. M. Tour, *Tetrahedron Lett.*, 2004, **45**, 2801–2803.
- 47 P. Hume, D. P. Furkert and M. A. Brimble, *Tetrahedron Lett.*, 2012, **53**, 3771–3773.
- 48 M. A. V. Ribeiro Da Silva, M. J. S. Monte, I. M. Rocha and L. Cimas, *J. Org. Chem.*, 2012, **77**, 4312–4322.
- 49 Y. Koizumi, M. Ide, A. Saeki, C. Vijayakumar, B. Balan, M. Kawamoto and S. Seki, *Polym. Chem.*, 2013, **4**, 484.
- 50 M. C. Yuan, M. Y. Chiu, C. M. Chiang and K. H. Wei, *Macromolecules*, 2010, **43**, 6270–6277.
- 51 B. C. Thompson and J. M. J. Fréchet, *Angew. Chem., Int. Ed.*, 2008, **47**, 58–77.

- 52 W. Huang, M. Li, L. Zhang, T. Yang, Z. Zhang, H. Zeng, X. Zhang, L. Dang and Y. Liang, *Chem. Mater.*, 2016, **28**, 5887–5895.
- 53 N.-K. Kim, S. Jang, G. Pace, M. Caironi, W.-T. Park, D. Khim, J. Kim, D. Kim and Y. Noh, *Chem. Mater.*, 2015, **27**, 8345–8353.
- 54 Y. Yuan, G. Giri, A. L. Ayzner, A. P. Zoombelt, S. C. B. Mannsfeld, J. Chen, D. Nordlund, M. F. Toney, J. Huang and Z. Bao, *Nat. Commun.*, 2014, **5**, 3005.
- 55 A. K. K. Kyaw, D. HwanWang, V. Gupta, W. L. Leong, L. Ke, G. C. Bazan and A. J. Heeger, *ACS Nano*, 2013, **7**, 4569–4577.
- 56 S. R. Cowan, A. Roy and A. J. Heeger, *Phys. Rev. B: Condens. Matter Mater. Phys.*, 2010, **82**, 245207.
- 57 N. Zhou, H. Lin, S. J. Lou, X. Yu, P. Guo, E. F. Manley, S. Loser, P. Hartnett, H. Huang, M. R. Wasielewski, L. X. Chen, R. P. H. Chang, A. Facchetti and T. J. Marks, *Adv. Energy Mater.*, 2014, **4**, 1300785.
- 58 X. Yang, J. Loos, S. C. Veenstra, W. J. H. Verhees, M. M. Wienk, J. M. Kroon, M. A. J. Michels and R. A. J. Janssen, *Nano Lett.*, 2005, **5**, 579–583.
- 59 L. J. A. Koster, V. D. Mihailetschi, H. Xie and P. W. M. Blom, *Appl. Phys. Lett.*, 2005, **87**, 1–3.
- 60 C. M. Proctor, M. Kuik and T. Nguyen, *Prog. Polym. Sci.*, 2013, **38**, 1941–1960.
- 61 L. Ye, X. Jiao, M. Zhou, S. Zhang, H. Yao, W. Zhao, A. Xia, H. Ade and J. Hou, *Adv. Mater.*, 2015, **27**, 6046–6054.
- 62 A. K. K. Kyaw, D. H. Wang, V. Gupta, W. L. Leong, L. Ke, G. C. Bazan and A. J. Heeger, *ACS Nano*, 2013, **7**, 4569–4577.
- 63 H. K. H. Lee, Z. Li, I. Constantinou, F. So, S. W. Tsang and S. K. So, *Adv. Energy Mater.*, 2014, **4**, 1–8.
- 64 W. L. Leong, S. R. Cowan and A. J. Heeger, *Adv. Energy Mater.*, 2011, **1**, 517–522.
- 65 J. C. Bijleveld, V. S. Gevaerts, D. Di Nuzzo, M. Turbiez, S. C. J. Mathijssen, D. M. De Leeuw, M. M. Wienk and R. A. J. Janssen, *Adv. Mater.*, 2010, **22**, 3–7.